

## The characteristics of the magnetopause reconnection X-line deduced from low-altitude satellite observations of cusp ions

M. Lockwood<sup>1</sup>, T.G. Onsager<sup>2</sup>, C.J. Davis<sup>1</sup>, M.F. Smith<sup>3</sup> and W.F. Denig<sup>4</sup>.

**Abstract.** We present an analysis of a "quasi-steady" cusp ion dispersion signature observed at low altitudes. We reconstruct the field-parallel part of the Cowley-D ion distribution function, injected into the open LLBL in the vicinity of the reconnection X-line. From this we find the field-parallel magnetosheath flow at the X-line was only  $20 \pm 60 \text{ km s}^{-1}$ , placing the reconnection site close to the flow streamline which is perpendicular to the magnetosheath field. Using interplanetary data and assuming the subsolar magnetopause is in pressure balance, we derive a wealth of information about the X-line, including: the density, flow, magnetic field and Alfvén speed of the magnetosheath; the magnetic shear across the X-line; the de-Hoffman Teller speed with which field lines emerge from the X-line; the magnetospheric field; and the ion transmission factor across the magnetopause. The results indicate that some heating takes place near the X-line as the ions cross the magnetopause, and that sheath densities may be reduced in a plasma depletion layer. We also compute the reconnection rate. Despite its quasi-steady appearance on an ion spectrogram, this cusp is found to reveal a large pulse of enhanced reconnection rate.

### Introduction

Recent models of cusp ion precipitation have demonstrated some important principles of how magnetosheath plasma gains access to the ionosphere along newly-opened field lines, produced by reconnection at the dayside magnetopause [Onsager *et al.*, 1993; Lockwood and Smith, 1994]. Once the field line is open, the ions stream continuously across the magnetopause. These ions have access to the ionosphere along each newly-opened field line until it is appended to the tail lobe. The velocity filter effect [Rosenbauer *et al.*, 1975; Hill and Reiff, 1977] arises because cusp ions of different field-aligned velocity, injected simultaneously across the magnetopause onto any one field line, have different flight times along that field line. Hence they have different arrival times in the ionosphere and, as the field line is convecting, are spatially dispersed along the locus of the field line. Figure 1 shows a typical dispersion signature for an equator-

ward-moving satellite for steady poleward convection and/or a steadily equatorward-eroding open/closed field line boundary [Lockwood and Smith, 1992]. The dashed lines connect ions which are injected across the magnetopause at the same place ( $P_n$ , which each field line reaches at a time  $t_n$  after it is opened) and are given by the time-of-flight relation:

$$d_n(m/2E)^{1/2} = t_s - (t_o + t_n) = t_s(1 - V_s/V_C) - t_n \quad (1)$$

where  $m$  and  $E$  are the ion mass and energy,  $d_n$  is the distance along the field line from  $P_n$  to the satellite, and  $V_C$  and  $V_s$  are the convection and satellite speeds normal to the open-closed boundary, OCB (both in the OCB rest frame and both defined as positive poleward). A field line opened at a time  $t_o$  is observed at a time  $t_s$  (in fig. 1 defined as zero at the OCB where  $t_s = t_o$ ) at a distance  $V_s t_s = V_C t_o$  poleward of the OCB. Ions begin to enter the magnetosphere along each newly-opened field line near the X-line, where  $t_n$  has a minimum value of  $t_n = 0$ , which by equation (1) yields a minimum  $E$  called the "lower cut-off" energy,  $E_{ic}(t_s)$ . In other words, the lowest energy ions seen at any one  $t_s$  have the longest flight time and were the first to be injected (and thus were injected close to the X-line). In figure 1,  $P_1$  is at the X-line and  $E_{ic}$  is shown as the lower part of the solid line. The dashed line labelled  $P_1$  corresponds to the energies and arrival times of ions injected at the reconnection X-line, a distance  $d_1$  from the satellite.

The theory of Cowley [1982] predicts that ions injected into the open low-latitude boundary layer (LLBL) will have a D-shaped ion velocity distribution function. This prediction has recently been verified in considerable qualitative and

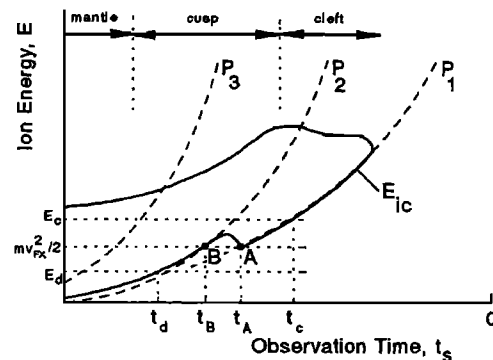


**Figure 1.** Schematic of cusp ion precipitation observed by an equatorward-moving satellite ( $V_s < 0$ ) for poleward convection ( $V_C > 0$ ). The solid line shows the limits of detectable magnetosheath ion fluxes (the lower limit being the low-energy cut-off,  $E_{ic}$ ) as a function of observation time  $t_s$ . The dashed lines connect ions injected at the same points ( $P_1$ ,  $P_2$  and  $P_3$ ) at the magnetopause. The X-line is at  $P_1$  where the field lines evolve along the magnetopause at a de-Hoffman Teller velocity of  $V_{HT}$ .

<sup>1</sup>Rutherford Appleton Laboratory, Chilton, Oxon., UK.

<sup>2</sup>Institute for the Study of the Earth, Oceans, and Space and Department of Physics, University of New Hampshire, USA.

<sup>3</sup>Laboratory for Extraterrestrial Physics, Goddard Space Flight Center, Greenbelt, Maryland, USA.

<sup>4</sup>Phillips Laboratory, Hanscom AFB, Bedford, Massachusetts, USA.

Copyright 1994 by the American Geophysical Union.

Paper number 94GL02696

0094-8534/94/94GL-02696\$03.00

quantitative detail by Gosling [1990], Smith and Rodgers [1991] and Fuselier *et al.* [1991]. The minimum speed of these injected ions will be very close to  $V_F$ , the de-Hoffman Teller velocity [Smith and Rodgers, 1991]. At the X-line this has a value of  $V_{FX}$ , and the ions from the X-line are dispersed along the dashed line marked  $P_1$ , but only down to A, which is at the minimum injected energy of  $(mV_{FX}^2/2)$  and which the satellite intersects at a time  $t_A$ . Lockwood and Smith [1994] have shown that, as each newly-opened field line evolves from the X-line to the tail lobe, the minimum injected energy firstly rises (as the field line accelerates) and then falls near the magnetic cusp (as it straightens). In figure 1, the minimum energy of ions injected across the magnetopause does not fall back to  $(mV_{FX}^2/2)$  until the source point  $P_2$ . Ions from  $P_2$  are dispersed along the dashed line labelled  $P_2$  down to the point B, encountered by the satellite at time  $t_B$ . For  $t_B < t_s < t_A$  the cut-off ion energy,  $E_{ic}$  exceeds  $(mV_{FX}^2/2)$ .

Figure 1 shows that at an energy  $E_d < (mV_{FX}^2/2)$ , the equatorward-moving satellite will observe a low energy cut-off ( $E_d = E_{ic}$ ) at a time  $t_d < t_B$  while at an energy  $E_c > (mV_{FX}^2/2)$ , it will observe it at  $t_c > t_A$ . At an energy just greater than  $(mV_{FX}^2/2)$ , the satellite will observe the cut-off three times and there will be a local minimum in the ion distribution function,  $f(v)$ , between  $t_B$  and  $t_A$ . This set of features is used here to estimate  $t_A$ , and hence  $V_{FX}$ .

### Observations on 26 January 1984

We present an analysis of ion observations made by DMSP-F7 spacecraft as it traversed equatorward through the cusp on 26 January, 1984. This pass reveals a cusp plume of a type which Lockwood and Smith [1994] have pointed out reveals "quasi-steady" reconnection and which Onsager *et al.* [1993] have modelled using the concepts of a steady-state, open magnetosphere. Figure 2 shows the sequence of  $f(v)$  during this pass, which reveals that  $E_{ic}(t_s)$  rose with time, as in figure 1. However, ion scattering and aliasing (by changes in particle flux within the 1-s. instrument integration periods) make precise determination of  $E_{ic}(t_s)$  from  $f(v)$  difficult. To

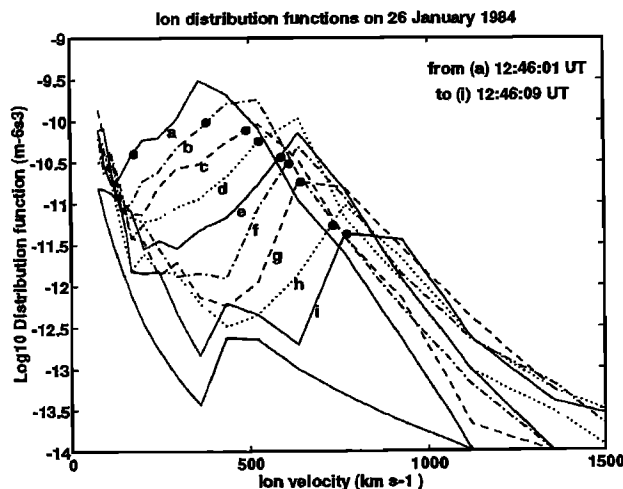


**Figure 2.** Sequential ion velocity distribution functions,  $f(v)$  observed by DMSP-F7 during a cusp crossing on 26 January 1984 between (a) 12:46:01 and (i) 12:46:09. Isotropic downward fluxes of protons are assumed. The lower solid line gives the one count level. Solid circles give the time-of-flight cut-off defined from fig. 3.

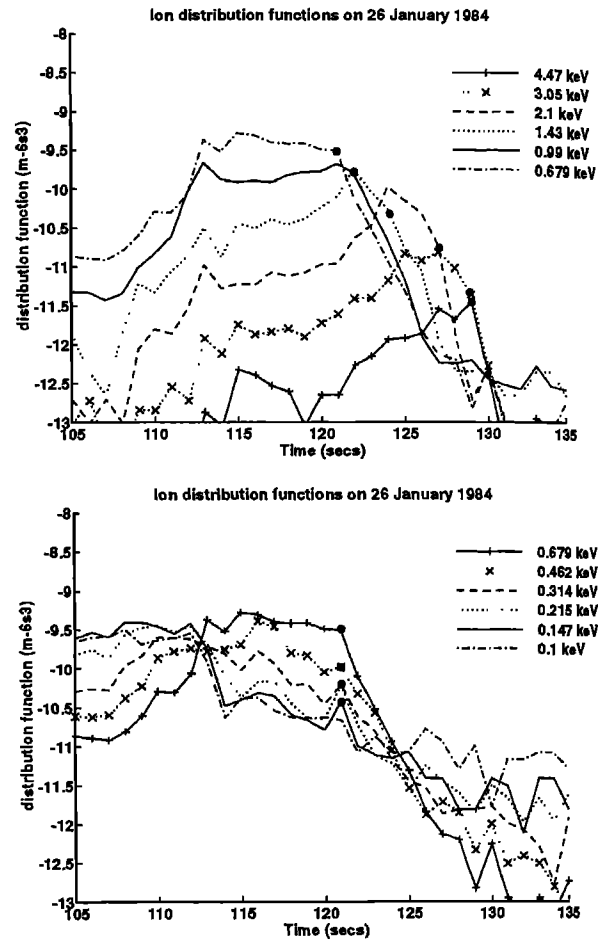


**Figure 3.** Time series of distribution function  $f(t_s)$  for each energy ( $E$ ) channel: (a) 679eV - 4.47keV (top); (b) 100eV - 679eV (bottom). The time  $t_s = 0$  is here defined to be 12:44.

make a better estimate of  $E_{ic}$ , we here make use of the plots of  $f(t_s)$  at constant energy,  $E$  (figure 3). At all energies, a decay in  $f(t_s)$  is seen as the satellite emerges through the equatorward edge of the cusp. A clear onset of the decay (i.e. the last high value before the major decrease in  $f$ ) can usually be defined and, where not unambiguously clear, it can be found by reference to adjacent channels. For the higher energy channels (figure 3a), the decay occurs later for higher  $E$ , as expected: its onset is marked by a dot for each energy channel. Figure 3b shows the behaviour is more complex at lower energies. For  $E = 100$  eV, a clear decay is observed at  $t_s$  between 112s and 114s ( $t_s = 0$  is here defined at a reference time of 12:44, not the OCB): subsequently,  $f$  remains at an intermediate level before decaying gradually, which we attribute to higher-energy ions scattered to lower energies. The same sort of behaviour is seen at  $E = 147$  eV, but with a small peak at  $t_s = 121$  s, which is also observed at 215 eV and 314 eV. At  $E$  of 462 eV and above, the onset of the decay is after  $t_s = 121$  s. This is exactly as predicted in figure 1, with the added complication of the scattered ions. We believe the small peak at  $t_s = 121$  s is significant because it occurs in three energy channels, but also because it is located at the end of the change in the onset time of the decay from  $t_s$  of 112 s to 121 s, as  $E$  rises from 100 eV to 314 eV. We identify the time  $t_A$  to be 121s (and  $t_B$  to be in the interval 114-117s). The lowest energy showing  $f$  above scattered

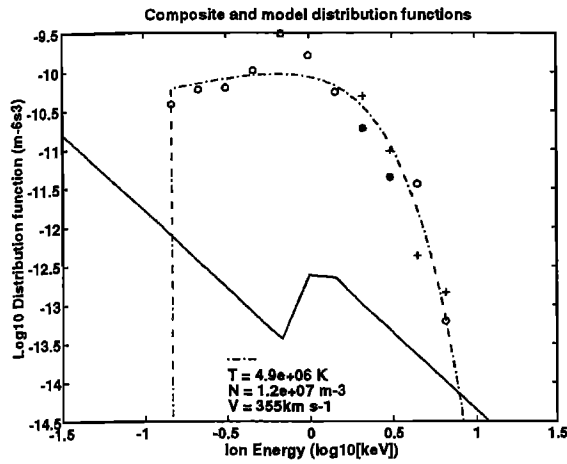


Figure 4. The Cowley-D distribution function in the (open) LLBL close to the X-line. The open circles are the values of  $f(E_{ic})$  which are obtained from the last data points before the decays in  $f(t_s)$ , shown in figure 3 by solid circles: at these points,  $E$  is taken to be sufficiently close to  $E_{ic}$  that  $f = f(E_{ic})$ . The crosses are peaks of  $f(v)$  where that peak and the noise level are just one energy channel apart. The solid line is the one-count level. The dot-dash line is the least-squares fit to these data points of a truncated, drifting Maxwellian.

values at the time  $t_A$  is 147 eV. Below this energy the decay in  $f$  is before  $t_B$ , whereas above it the decay is after  $t_A$ . The minimum in  $f$  between  $t_B$  and  $t_A$  is weak because of scattering, but is clearly present in 3 energy channels. Hence we can identify the energy of A and B (figure 1) to be  $147 \pm 40$  eV, giving  $V_{FX} = 168 \pm 30$  km s<sup>-1</sup>, which is typical of the results from magnetopause stress-balance tests [e.g. *Smith and Rodgers*, 1991]. In figure 3, only the cut-offs for  $t_s > t_A$  (i.e. ions from near the X-line) are marked by dots.

The cut-offs derived from figure 3 are also shown in figures 2 and 4, and can be seen to describe a drifting Maxwellian. Figure 2 demonstrates that the cut-off bears no fixed relationship to the peak. This is to be expected because the peak  $f$  at any one  $t_s$  is due to ions injected when the field line has evolved away from the X-line (where the cut-off ions are injected). On crossing the magnetopause at this later time, the ions are not so strongly accelerated, making  $f$  larger inside the magnetosphere for energies where  $df/dE$  is positive. This effect is partly compensated by changes in the density and temperature in the sheath, but still results in  $f(E_{ic})$  being smaller than the peak  $f$  if  $E_{ic}$  is low. Hence the peak  $f$  should not be used to define  $E_{ic}$ . The only exception to this is for those  $t_s$  when  $f$  rises from the noise level to the peak in adjacent energy channels because  $df/dE$  is negative. The peak  $f$  is then a good estimate of  $f(E_{ic})$  and these are given as crosses in figure 4. For adiabatic, scatter-free motion between the X-line and the ionosphere,  $f$  (by Liouville's theorem) and  $E$  are conserved. Hence, because it is taken from our best estimate of the dashed line  $P_1$  in figure 1, figure 4 is a reconstruction of the field-parallel part of the Cowley-D distribution in the open LLBL close to the X-line. This procedure is similar to that employed by *Hill and Reiff* [1977] but different because it is here applied to the cut-off, rather than the peak of the  $f(v)$ . The dot-dash line gives a least-squares fit, from which we find that the population in the open LLBL near the X line has a field-aligned bulk drift

$V_{pX} = 355 \pm 15$  km s<sup>-1</sup>, a parallel temperature  $T_{||} = 4.9 \times 10^6$  K and a density,  $N = N_{||}A = 12A$  cm<sup>-3</sup>, where  $A$  is the temperature anisotropy,  $T_{\perp}/T_{||}$  [see *Hill and Reiff*, 1977]. The minimum energy is placed at 147 eV, as inferred above. The two poorly-fitted points are for when both  $E_{ic}$  and  $f(E_{ic})$  changed rapidly near  $t_s = 121$ s: hence, although they were given equal weight in the fitting procedure, we believe they are the most in error due to time aliasing.

The IMP-8 satellite made observations of the solar wind at this time and taking an average of the (relatively steady) values for 12:35-12:45, which allows for the estimated IMP-8 to magnetopause propagation delay, we obtain X, Y and Z components of the IMF of -0.78, -2.99 and -2.21 nT, respectively. The solar wind had density  $N_{sw}$  of 11 cm<sup>-3</sup>, temperature  $T_{sw}$  of  $2 \times 10^5$  K and flow speed  $V_{sw}$  of 385 km s<sup>-1</sup>.

### Conditions at the reconnection site

The theory of *Cowley* [1982] shows the field-aligned sheath flow velocity at the X-line in the Earth's frame,  $V_{shX}$ , is equal to  $(2V_{FX} - V_{pX})$ . From the above values we find  $V_{shX}$  to be  $-19 \pm 62$  km s<sup>-1</sup>. Such a low sheath speed is highly significant, as it tells us that the reconnection site must be very close to the stagnation region at the nose of the magnetosphere, or be closely aligned with the flow streamline which is orthogonal to the magnetosheath field: in either case the field-aligned sheath flow is close to zero and there is little flow perpendicular to the X-line. The theory also yields the Alfvén speed in the magnetosheath, in the vicinity of the X-line  $V_{AX} = (V_{pX} - V_{FX}) = 187 \pm 34$  km s<sup>-1</sup>. If we define the fraction of the sheath density that enters the LLBL to be  $R = N/N_{sh}$ , and assume the magnetopause to be in equilibrium, then we can equate the solar wind dynamic pressure with the thermal and magnetic pressures in the sheath, giving:

$$R = (N_{||}A/N_{sw})(kT_{sh}/m + V_{AX}^2/2)/(cV_{sw}^2) \quad (2)$$

where  $c$  is the term for Newtonian pressure balance with a blunt-nose magnetosphere, which is 0.84 at the nose, and decreases as  $\cos^2 i$  [*Spreiter et al.*, 1966]. (We here take  $i$ , the angle between  $V_{sw}$  and the magnetopause normal, to be zero because the observations are close to magnetic noon). In modelling all injected ions in this cusp pass, *Onsager et al.* [1993] employed solar wind values very close to those observed by IMP-8, but with a density which was too low by a factor 2.5, implying either that sheath densities are reduced in a plasma depletion layer and/or that their assumed  $R$  of 0.5 was too high: this could yield  $R$  as low as 0.2, which is

Table 1. Derived X-line parameters for ion anisotropy,  $A = T_{\perp}/T_{||}$ , and magnetopause heating factor,  $T_{||}/T_{sh}$

A	$T_{\perp}/T_{sh}$	R	$N_{sh}$ (cm <sup>-3</sup> )	$B_{sh}$ (nT)	$B_{shz}$ (nT)	$\Delta B_z$ (nT)
1.0	1.0	0.50	24	42	-25	101
1.4	1.0	0.89	19	37	-22	98
1.50	1.0	1.00	18	36	-21	97
1.0	1.5	0.38	31	48	-28	104
1.4	1.5	0.67	25	43	-25	101
1.78	1.5	1.00	21	40	-24	100
1.0	2.0	0.33	37	52	-31	107
2.00	2.0	1.00	24	42	-25	101

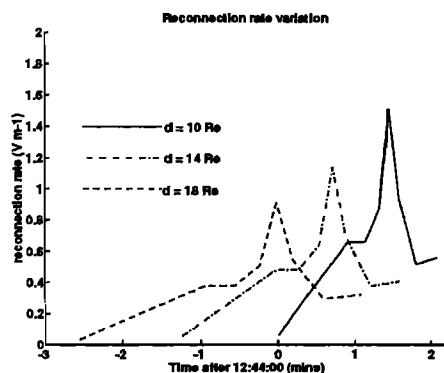


**Figure 5.** The reconnection rate variation from  $E_{ic}(t_s)$  for assumed satellite to X-line distances,  $d_j$ , of 10, 14 and  $18R_E$ .

slightly lower than the values observed by *Fuselier et al.* [1992] but slightly larger than recent estimates by *Onsager et al.* [1994]. *Onsager et al.* [1993] employed a gas-dynamic sheath model with a solar wind proton temperature of  $2 \times 10^5$  K, giving a temperature of  $T_{sh} = 4.2 \times 10^6$  K at the nose. This is slightly less than  $T_{||}$  derived in figure 4, implying that there may be some weak heating of the ions on crossing the magnetopause close to the X-line. Hence we also have considered various values of the ratio  $T_{||}/T_{sh}$ .

For assumed values of  $A$  and  $T_{||}/T_{sh}$  we can use (2) to estimate  $R$  and hence the magnitude of the magnetosheath field near the X-line,  $B_{sh} = V_{Ax}(\mu_0 m N_{||} A/R)^{0.5}$  and, because the IMF clock angle is conserved, this gives its Z-component  $B_{shz}$ . From pressure balance we can also estimate the internal field,  $B_{sp} = V_{sw}(2\mu_0 m c N_{sw})^{0.5} = 76$  nT. If we assume that this field points northward, this gives the z-component of the magnetic shear across the magnetopause of  $\Delta B_z = (B_{sp} + B_{shz})$ .

Table 1 gives the derived values for various assumed values for the anisotropy  $A$  and heating factor  $T_{||}/T_{sh}$ . The  $R$  in Table 1 is for field lines in the vicinity of the X-line and may not apply elsewhere on the magnetopause. The requirement that  $R < 1$  sets an upper limit to  $A$  which depends on  $T_{||}/T_{sh}$ . It is useful to compare the inferred  $N_{sh}$  with the value of  $17 \text{ cm}^{-3}$  employed by *Onsager et al.* [1993] (for  $R = 0.5$ ), but which would be raised to  $42 \text{ cm}^{-3}$  (for  $R = 0.2$ ) to get best agreement with the IMP-8 data. From Table 1, such a combination of high  $N_{sh}$  and low  $R$  also implies some heating (such that  $T_{||}/T_{sh} > 1$ ) and/or that  $N_{sh}$  is lower in a plasma depletion layer: the degree of depletion is limited, however, because of the limits placed on  $A$  [see discussion and references in *Hill and Reiff*, 1977] by  $R < 1$ .

Lastly, from the variation of  $E_{ic}(t_s)$  for  $t_s > t_A$  we are able to compute the reconnection rate as a function of time, using the equations of *Lockwood and Smith* [1992]. The results are shown in figure 5 for three assumed  $d_j$ , the field-aligned distance from the X-line to the satellite. Unit length on the X-line is mapped into the ionosphere as  $B^{-1/2}$ , using the value of  $B_{sp}$  derived above with an ionospheric field of  $5 \times 10^5$  T. It is assumed that the angle between the satellite path and the ionospheric flow streamline is small. The average reconnection rate is then 0.72, 0.53 and  $0.42 \text{ V m}^{-1}$  for  $d_j$  of 10, 14 and  $18R_E$ , respectively, giving mean flow speeds of flux tubes across the open/closed boundary (in the boundary rest frame),  $\langle V' \rangle$ , of 588, 434 and  $342 \text{ m s}^{-1}$ : the peak reconnection rate corresponds to peak  $V'$  of 1.24, 0.93 and  $0.74 \text{ km s}^{-1}$ .

Given that this pass is in the summer hemisphere and near the solstice, we would expect the inferred location of the reconnection site to give  $d_j$  near the lower end of the illustrative range employed here. Figure 5 shows that the reconnection rate is highly pulsed in this example, despite its relatively smooth (step-free) ion dispersion signature. *Lockwood and Smith* [1994] noted that fluctuations in the rate by a factor of as much as 2 would produce little detectable effect in the cusp ion dispersion signature, and hence predicted that even apparently "quasi-steady" dispersed cusp plumes may, in fact, be due to pulsed reconnection. Figure 5 shows this to be the case in the example presented here.

We note that the  $E_{ic}(t_s)$  profile used here to define  $V_{FX}$  is quite common in dispersed cusp plumes and hence our analysis could be used with a significant number of cusp passes.

**Acknowledgements.** ML and CJD are supported by the UK Particle Physics and Astronomy Research Council and MFS by NASA. TGO was supported by NASA grant NAGW-2505 and NSF grant ATM-9111754 and WFD at the Phillips Laboratory (program element 62101F, project 7601) and by AFOSR (program element 61102F, task 2311G5).

## References

- Cowley, S.W.H., The causes of convection in the Earth's magnetosphere: A review of developments during IMS, *Rev. Geophys.*, **20**, 531, 1982.
- Fuselier, S.A., D.M. Klumpar, and E.G. Shelley, Ion reflection and transmission during reconnection at the Earth's subsolar magnetopause, *Geophys. Res. Lett.*, **18**, 139, 1991.
- Gosling, J.T., et al., Cold ion beams in the LLBL during accelerated flow events, *Geophys. Res. Lett.*, **17**, 2245, 1990.
- Hill, T.W. and P.H. Reiff, Evidence of magnetospheric cusp proton acceleration by magnetic merging at the dayside magnetopause, *J. Geophys. Res.*, **82**, 3623-3628, 1977.
- Lockwood, M., and M.F. Smith, The variation of reconnection rate at the dayside magnetopause and cusp ion precipitation, *J. Geophys. Res.*, **97**, 14,841, 1992.
- Lockwood, M., and M.F. Smith, Low- and mid-altitude cusp particle signatures for general magnetopause reconnection rate variations: I - Theory, *J. Geophys. Res.*, **99**, 8531-8555, 1994.
- Onsager, T.G., et al., Model of magnetosheath plasma in the magnetosphere: cusp and mantle precipitations at low altitudes, *Geophys. Res. Lett.*, **20**, 479, 1993.
- Onsager, T.G., et al., Low-altitude observations and modelling of quasi-steady reconnection, *J. Geophys. Res.*, in press, 1994.
- Rosenbauer, H., et al., HEOS-2 plasma observations in the distant polar magnetosphere: the plasma mantle, *J. Geophys. Res.*, **80**, 2723, 1975.
- Smith, M.F. and Rodgers, D.J., Ion distributions during the dayside magnetopause, *J. Geophys. Res.*, **95**, 11,617, 1991.
- Spreiter, J.R. et al., Hydromagnetic flow around the magnetosphere, *Planet. Space Sci.*, **14**, 223-253, 1966.

C.J. Davis and M. Lockwood, RAL, Chilton, Didcot, OX11 0QX, UK. (e-mail: Internet. mike@eiscat.ag.rl.ac.uk)

W.F. Denig, Phillips Laboratory, PL/GPSG, Hanscom AFB, Bedford, MA01731-5000, USA.

M. F. Smith, Laboratory for Extraterrestrial Physics, NASA Goddard Space Flight Center, Greenbelt, MD 20771, USA.

T.G. Onsager, Space Science Center, University of New Hampshire, Durham, NH 03824, USA.

(Received July 15, 1994; revised August 19, 1994; accepted September 23, 1994.)